Ethiopian Journal of Science and Sustainable Development

e-ISSN 2663-3205 *Volume 11 (2), 2024*

Journal Home Page: www.ejssd.astu.edu.et

Research Paper

Spatiotemporal analysis of land surface temperature and soil water stress in Erer Watershed of Wabi Shebelle River Basin, Ethiopia

Asfaw Kebede Kassa[1,*], Bekele Girma[2], Negash Tessema[2], Demelash Debebe[3]

[1]*Haramaya University, Department of Hydraulic and Water Resources Engineering, Dire Dawa, Ethiopia*
[2]*Haramaya University, Department of Water Resources and Irrigation Engineering, Dire Dawa, Ethiopia*
[3]*Water Resources and Irrigation Engineering Department, Woldia University, Woldia, Ethiopia*

Article Info

Article History:
Received 27 January 2024
Received in revised form 09 April 2024
Accepted 13 April 2024

Keywords:
Erer watershed,
LST,
NDVI,
Soil Moisture Index,
TVDI

Abstract

Understanding the land surface process in numerical models necessitates the consideration of Land Surface Temperature (LST) and soil moisture. LST plays a crucial role in regulating surface and sub-surface heat; thus, influencing water circulation within the atmosphere. This study utilized Landsat 8 Optical Land Imager (OLI) images with a 30 m resolution to analyze LST, Soil Moisture Index (SMI) and Vegetation Dryness Index (TVDI) for the Erer Watershed, which is in the Wabi Shebelle River basin in Ethiopia. The investigation spanned six years, from 2015 to 2021, and it involved determining the Normalized Difference Vegetation Index (NDVI) for each specified year to get LST, soil water stress, and TVDI. The thermal infrared band's digital values were converted into spectral radiance using the relation specified in the Landsat user's manual. The final LST was derived using surface emissivity based on NDVI classes. The findings revealed an increasing trend in LST, SMI, and TVDI over time, signifying decline in soil moisture. The north-eastern and north-western sections of the Erer Watershed exhibited the highest values of LST, SMI, and TVDI, with a negative correlation observed with soil moisture. The spatial distribution of LST, SMI, and TVDI can be used as a valuable reference for managing soil water stress and to understand ecosystem services. Additionally, LST may serve as a significant indicator in monitoring environmental changes, particularly in relation to drought, within the study area.

1. Introduction

Understanding the spatiotemporal dynamics of land surface temperature (LST) and soil water stress within a basin is essential for effective land and water resource management. Both LST and soil water stress play significant roles in regulating ecosystem health, agricultural productivity, and hydrological processes. LST regulates both surface and sub-surface heat dynamics, thereby influencing water circulation within the atmosphere. In numerical models of simulating Earth's surface processes, the integration of LST and soil moisture data is imperative to accurately represent the system. The continual decline in land use land cover on the earth's surface primarily stems from human activities, which constitute the majority of such alterations. The decrease in vegetation is a significant factor contributing to the rise in the LST. Vegetation emerges as the principal driver behind LST variations (Song et al., 2021). LST serves as a crucial metric for assessing ecological functionality, offering insights into earth's surface temperature vital for both local and global investigations (Phan et al., 2018). Globally, the upward trend in LST is attributed to shifts in land use

*Corresponding author, e-mail: asfaw649@gmail.com

https://doi.org/10.20372/ejssdastu:v11.i2.2024.824

and cover, leading to increased soil water stress and degradation (Mitiku et al., 2022; Sun and Pinker, 2003).

Conversely, water held within the pores of soil particles against gravity, expressed as soil moisture (SM), is a significant factor in hydrological management and sympathetic the energy balance of terrestrial water (Liu et al., 2012). Even when soil moisture is limited, it remains a crucial variable in global and regional climate scale models. Soil moisture, comprising less than 0.05 % of the planet's freshwater resources (Anderson and Croft, 2009; Li et al., 2021), is best gauged through direct ground-based methods for precise measurement. These approaches offer the most reliable assessment of soil water content (Dobriyal et al., 2012), ensuring consistency in evaluation.

Surface temperature is a pivotal parameter for applications in hydrology, meteorology, and climatology. It serves as a vital index in assessing the energy budget of the earth's surface. This parameter is crucial for determining the net radiation budget at the land surface, monitoring crop and plant health, and acting as a significant indicator of the impact of nurseries and the exchange of vitality between the atmosphere and the ground. The features of the land surface, such as green cover, land usage, and surface impermeability, influence LST, and variations in LST can impact soil water. LST offers essential insights into the physical characteristics and climate of the surface, playing a crucial role in various environmental contexts (Lu and Weng, 2004).

LST is influenced by various factors, including solar radiation, land cover, vegetation density, and soil moisture content. The presence of more greenhouse gases in the atmosphere has significantly worsened the magnitude of LST and reducing the soil moisture. Increase in LST also has an impact on the monsoon countries' weather, causing unpredictable rainfall (Rahman and Dedieu, 1994). This has an impact on soil moisture which causes soil-water stress. Estimating LST areas posed challenges before the advent of Earth Observation Satellites (EOS) (Khandelwal et al., 2018). A variety of methods have been used to analyze the spatiotemporal dynamics of LST and soil water stress in basins (Sobrino and Raissouni, 2000; Mitiku et al., 2022). Remote sensing techniques, including thermal infrared imagery and microwave radiometry, are commonly used to estimate LST and soil moisture content over large spatial extents. .

To transform point data into spatial data, LST was traditionally computed for precise sample points and then interposed into isotherms (Mallick et al., 2008). Isometric LST maps were commonly derived through spatial interposition techniques applied to observations at sample locations (Ali and Shalaby, 2012). Das et al. (2022) emphasized the substantial influence of land-use land-cover changes on LST, while Zullo et al. (2019) highlighted the impact of the spatial pattern of urban expansion on LST. These issues led to numerous research projects focusing on soil water (SM) and LST. Temperature Vegetation Dryness Index (TVDI) and Soil Moisture Index (SMI methods stand out as widely employed synergistic techniques for soil moisture analysis (Sobrino and Raissouni, 2000). Utilizing the Normalized Difference Vegetation Index (NDVI) and LST, TVDI and SMI provide approximations of soil moisture or dryness (Sandholt et al., 2002). Given its role in the energy exchange between the land surface and the atmosphere, LST is a crucial metric for assessing surface soil moisture (Wan et al., 2004).

Examining terrain effects on land surfaces often relies on satellite imagery, which provides valuable insights into land cover and patterns, including vegetation, water bodies, bare soil, and more (He and Wu, 2019). Currently, the geographical detection of LST is facilitated by satellites equipped with high-resolution sensors. By utilizing thermal ultraviolet bands available on satellites, like Landsat, it becomes feasible to compute LST for entire areas in a single analysis. Several scholars have utilized Landsat imagery to create land use or cover images. However, remotely sensing land surfaces poses significant challenges due to the vast variability of land surfaces and complexities in eliminating atmospheric influences. Additionally, there exists a disparity between the criteria for land surface models and remote sensing, where remote sensing assesses emissivity through channels at specific wavelengths (Sobrino et al., 2004).

Studies conducted in various regions of Ethiopia (Mitiku et al., 2022; Bayisa et al., 2022; Dissanayake et al., 2019) indicated a substantial increase in LST. Specifically, Mitiku et al. (2022) showed increase in LST by 9.5 °C over 30 years period (1990 to 2020).

Similar to LST, soil water stress, temperature dryness, changes in land-use and land-cover are causing a large increase in air temperature (Dessalegn et al., 2021; Mitiku et al., 2022). One of the most used water stress indices for determining soil water stress using LST and NDVI distributions are TVDI and SMI. To assess the ambient environmental conditions suitable for living organisms, NDVI offers a more comprehensive evaluation compared to LST. Additionally, the necessity of representing the distribution of green space has been supported by the use of NDVI (Yuan and Bauer, 2007). A gradual decline in remote detection indicators, including NDVI and Modified Normalized Difference Water Index (MNDWI) are documented (Liang et al., 2011; Vlassova et al., 2014). This decrease is attributed to various factors such as disforestation, heightened urbanization, forest fires, the expansion of cultivable land, and the enlargement of pasture lands. The decline in the indices is associated with an increase in LST.

Although the indices have been utilized in prior research to model LST (Chen and Zhang, 2017), a limited number of studies have undertaken a comparison of index data from different time series data for assessing surface temperature. In Eastern Ethiopia, where LST is a significant contributor to climate change, the impact of this phenomenon has repercussions on the agricultural development in the region. It is clear that the decrease in the amount of natural cover for agricultural development is what has caused the LST to increase over time. The decline of wetlands and the spread of parched land were other reasons causing an increase in LST. Thus, understanding LST and soil water stress spatial patterns and their drivers is crucial for informed land management decisions, agricultural planning, water resource allocation, and climate change adaptation strategies within the basin.

Moreover, despite advances in remote sensing technologies and spatial analysis techniques, several knowledge gaps persist in the spatiotemporal analysis of LST and soil water stress in basins. There is a need for improved spatial resolution and accuracy of remote sensing data, especially in heterogeneous landscapes and complex terrain. Besides, detailed research is required to understand the interactions between LST, soil moisture, vegetation dynamics, and hydrological processes at finer temporal scales, including diurnal and seasonal variations. Integrated interdisciplinary approaches, combining remote sensing, and climate factors, are essential for advancing the understanding of the complex spatiotemporal dynamics of LST and soil water stress in basins and their implications for sustainable land and water management. Therefore, this study used remote detection indicators like NDVI, SMI, and TVDI to examine LST and soil water stress in Erer Watershed.

2. Materials and Methods

2.1. Description of the study area

This study focused on Erer Watershed, which is in the Upper Wabi Shebelle Basin, a vital transboundary river basin in East Africa, particularly Ethiopia. The Sub-basin is situated between 08°12'35" and 09°31'07" N latitude and 42°04'27" and 42°31'07" E longitude (Figure 1), with elevation ranging from 800 to 2,920 m.a.s.l. and drainage area of 3,860 km^2. It is predominantly characterized by Kolla (warm semiarid) climate; approximately 73.5% of the Erer Watershed falls within an elevation range of 500 to 1500 m above sea level. The Woina Dega (cool sub-humid; 1500–2300 m.a.s.l.) and Dega (cool humid; 2300–3200 m.a.s.l.) climates constitute around 25.12 and 1.36% of the total drainage area, respectively. The catchment experiences annual variations in average rainfall, ranging between 744 and 1017 mm; the majority of the rainfall occurs during summer (Shumete, 2015). The climatic variations within the Erer Watershed provide a diverse and dynamic backdrop for the study's exploration of environmental factors and patterns.

The average maximum temperature for a given month is 29.95°C, and the mean minimum temperature is 16.72°C. The principal soil types, which make up 4, 8, 20, 19, 49 and 16%, respectively, of the entire research area, are humic cambisols, dystric cambisols, eutric nitosols, eutric regosols, haplic xerosols and calcaric regosols (MoA, 2000).

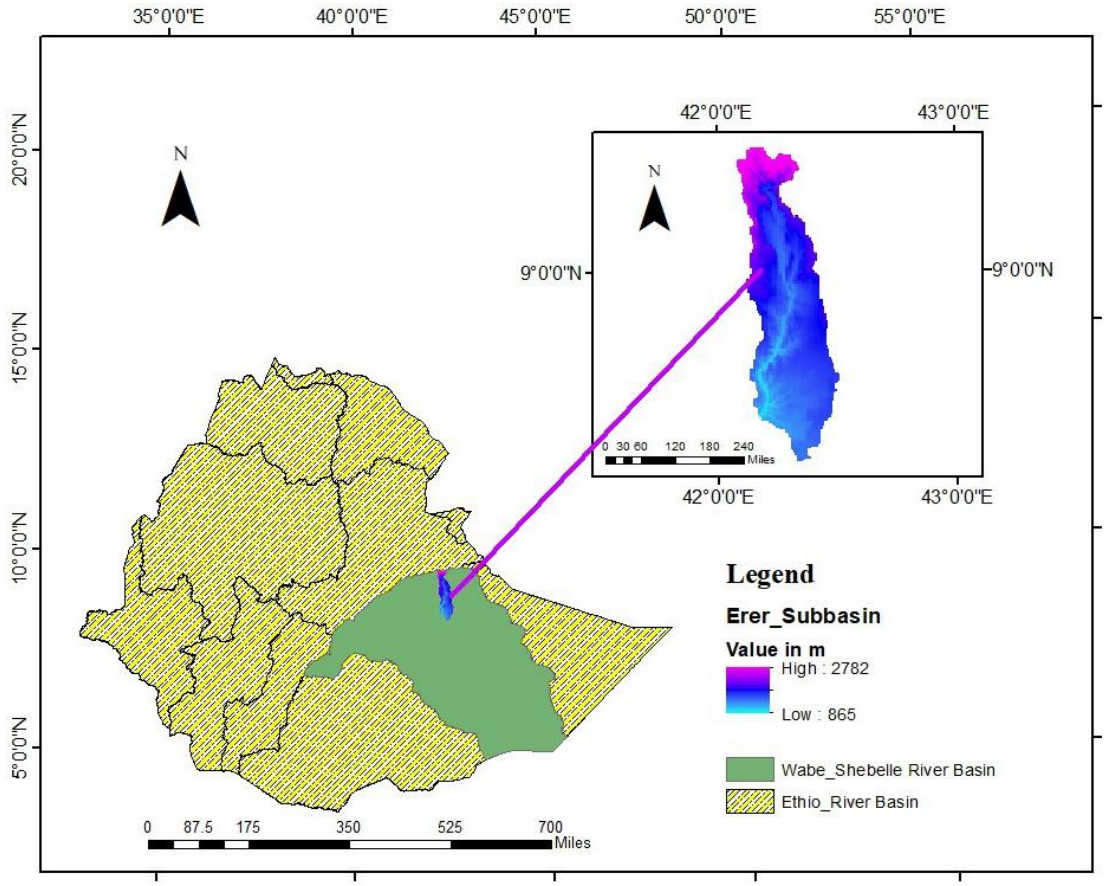

Figure 1: Ethiopian River basin and study area location

2.2. Data Collection and processing

The Landsat 8 images used to cover Erer Watershed were obtained through the USGS Earth Explorer's online data services (USGS, 2021). The image was captured during periods of ten percent or low cloud cover throughout the dry and wet seasons. Accordingly, landsat8 sensors of accuracy 30 m and bands 4-11, acquired on Dec. 15, 2015 and Dec. 15, 2021, were employed to map the LST in Erer Watershed. The wet months in Erer Watershed last from May - October, and the dry season lasts from November - April. Image correction and preprocessing were performed using the standard procedure as explained below.

The pre-processing of the images encompassed both visual and digital image processing. Specifically, for further analysis, bands of B10 and B11 from the thermal infrared spectrum were selected. Area of interest was selected using Erer Watershed shape file that was extracted from the complete scenes. ERDAS imagine 2015 software were used for image processing.

Corrections were applied to the images to rectify potential distortions introduced during image collection process, utilizing toolbox developed by the European Union's Joint Research Centre. Geocoding was implemented using the coordinate and mapping system derived from national topographic maps to guarantee precise identification of changes over time and to maintain geometric compatibility with other data sources. UTM zone 37 North coordinate system were used to project all images referencing WSG1984 for consistency.

2.3. Retrieval of land surface temperature (LST)

The image analysis process was performed using ArcGIS 10.4. In this investigation, Landsat 8's thermal infrared, two bands Band10 and Band11 were employed to determine brightness illumination temperatures, while Band 4 and Band 5 were utilized for estimating the NDVI. USGS web page sourced as LST query methods to save the peak of top of atmospheric (TOA)

spectral radiance (USGS, 2021). The retrieval of LST followed the steps outlined in Figure (2).

2.3.1 Top of Atmospheric Spectral Radiance

Using the radiance rescaling coefficients outlined in the metadata file, the digital numbers (DN) corresponding to the thermal band data underwent a transformation to top-of-atmosphere (TOA) spectral radiance, as described by Eq. (1) (Avdan and Jovanovska, 2016).

$$L\lambda = M_L * Q_{cal} + A_L \quad (1)$$

where $L\lambda$ = *TOA* (Watts/(m^2×srad×μm)), M_L = Band-specific multiplicative rescaling factor, Q_{cal} is quantized and calibrated standard product pixel values (DN), A_L = band-specific additive rescaling factor.

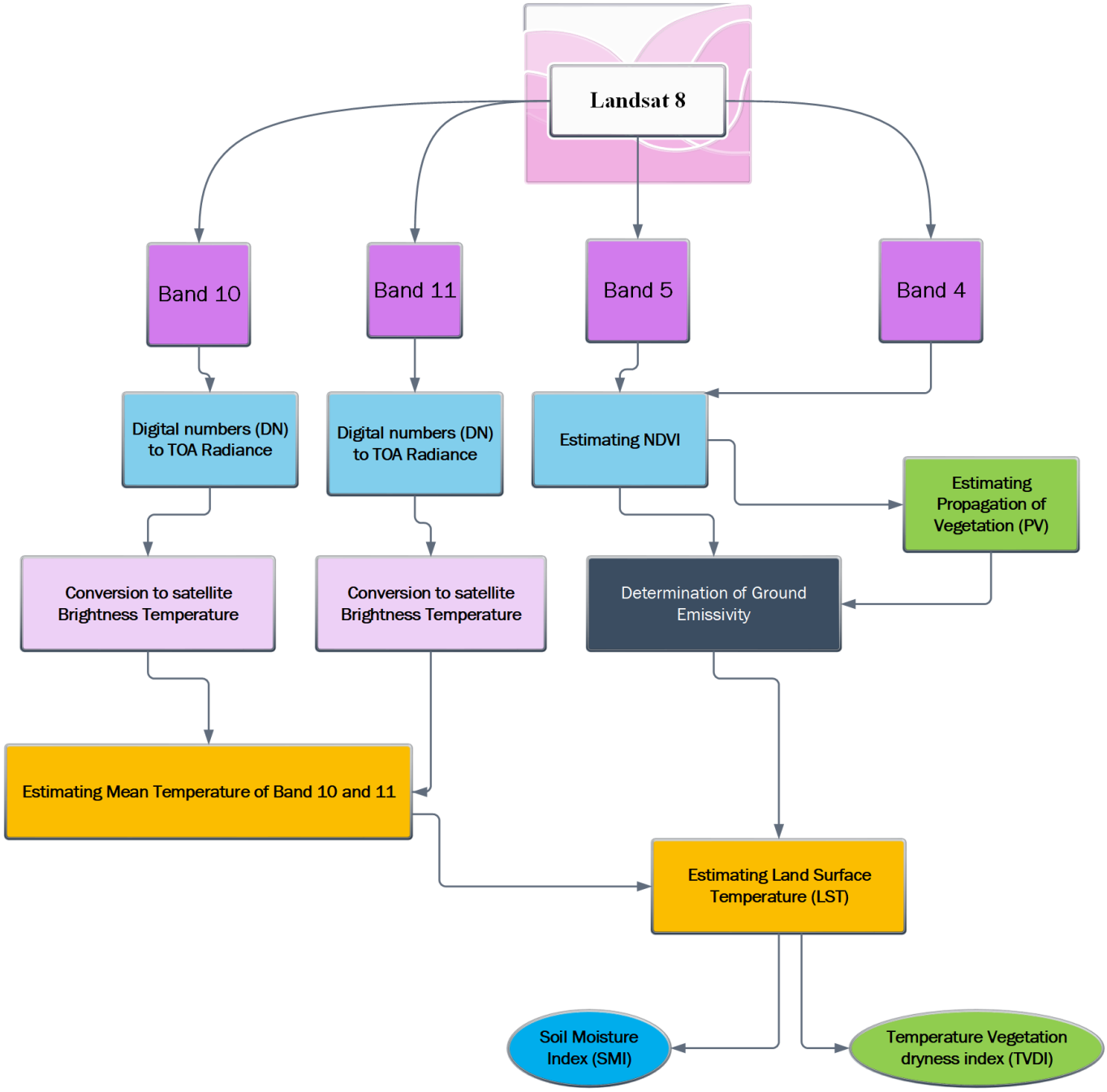

Figure 2: Flow chart used in the research

The thermal coefficients available in the Metadata file applied to convert thermal band data from spectral radiance to top of atmospheric illumination temperature (Avdan and Jovanovska, 2016). This is given as Eq. (2).

$$BT = \frac{K_2}{\ln[\left(\frac{K_1}{L\lambda}\right)+1]} - 273.1 \quad (2)$$

where: BT = TOA brightness temperature; K_1 and K_2 are band-specific thermal conversion constant from the metadata.

2.3.2 Estimation of NDVI values

Drought conditions are intricately linked with the NDVI derived remote sensing data. Diverse wavelengths of Red and near-infrared band (NIR) sunlight send back by green vegetation are analyzed to assess the green density on the watershed area. The estimation of the NDVI values involved the use of the red (B4) and NIR (B5) bands. As the quantity of green cover plays a pivotal role, and the NDVI serves as an indicator of overall vegetation status, the estimation of NDVI becomes imperative. Eq. (3) used for estimation of NDVI from Landsat 8 (OLITIRS).

$$\text{NDVI} = \frac{\text{B 5}-\text{B 4}}{\text{B 5}+\text{B4}} \quad (3)$$

2.3.3 Proportion of vegetation (P_V) estimation

The extent of land covered with green, as seen from a perpendicular perspective, is commonly referred to as the P_V value or the vegetation fraction. Changes in green cover significantly impact energy balances through processes such as plant transpiration, surface water retention, surface albedo, emissivity, and surface roughness. NDVI values, indicative of both vegetation and soil, are intricately linked to the P_V percentage of green cover. To estimate the proportion of green cover, the traditional NDVI approach (Rouse et al., 1974), given as Eq. (4), was employed.

$$\text{Pv} = \left(\frac{\text{NDVI}-\text{NDVIs}}{\text{NDVIv}-\text{NDVIs}}\right)^2 \quad (4)$$

where NDVIv is maximum NDVI for green-cover and NDVIs is minimum one for soil.

2.3.4 Estimation of land-surface Emissivity

Land-surface Emissivity (LSE or ε) is derived from earth surface temperature and radiance, representing mean emissivity of a surface element on land. As a crucial proportionality factor in scaling blackbody radiance to forecast released radiance, LSE plays a significant role in efficiently conveying thermal energy across the surface into the atmosphere. Knowledge of LSE is essential for estimating LST (Jimenez-Munoz et al., 2006). Based on Sobrino et al. (2004), ground emissivity is determined by Eq. (5).

$$\varepsilon_\lambda = \varepsilon_{v\lambda} P_V + \varepsilon_{S\lambda}(1 - P_V) + C_\lambda \quad (5)$$

where εv = vegetation emissivity;, εs = soil emissivity, C = surface roughness = 0.005 (Sobrino and Raissouni, 2000).

When NDVI is less than 0, it is classified as water and the corresponding emissivity rate is 0.991. For NDVI values within 0 and 0.2, the land is considered to be covered by soil, and 0.996 is applied as an emissivity value (Baris et al., 2014). For NDVI between 0.2 and 0.5, it is considered a combination of soil and green cover. When the NDVI value exceeds 0.5, vegetation is deemed present, and a value of 0.973 is given. An emissivity rate 0.996 is provided in this study, considering the typical NDVI range between 0 and 0.2.

Then, Eq. (6) (Baris et al., 2014), was used to estimate LST, or the emissivity modified earth surface temperature Ts.

$$Ts = \frac{BT}{1+[\left(\frac{\lambda BT}{C2}\right)ln\varepsilon\lambda]} \quad (6)$$

where Ts is LST in ^oC, BT = at-sensor brightness temperature ($^\circ$C), λ = the wavelength of emitted radiance (λ = 10.895) (Baris et al., 2014), C_2 = 1.4388 * 10^{-2} m K (Eq.13), ελ = the emissivity estimated above.

2.4. Soil moisture index (SMI)

In a number of earlier investigations, remote sensing was utilized to map soil moisture using techniques such as earth surface temperature (Amani et al., 2017; Mohamed et al., 2020) and the alteration of vegetation indicators (Joiner et al., 2019; Schnur et al., 2010). In this work, SMI is determined using the LST technique, and data on vegetation density is developed using

NDVI. The strongest relationship between NDVI and soil surface moisture is positive (Amani et al., 2017), and vegetation is the most important factor in determining soil moisture.

The soil moisture content (SWC) decreases as the green-cover increases (Yang et al., 2018). The state of LST is influenced by the energy balance of the surface, atmospheric conditions, thermal properties of the surface, and characteristics of the subsurface media (Weng, 2009). Low infiltration indicates significant soil moisture when the surface temperature is low (Saha et al., 2019). The SMI was estimated using the Eq. (7) (Saha et al., 2019).

$$\text{SMI} = \frac{\text{LSTmax} - \text{LST}}{\text{LSTmax} - \text{LSTmin}} \quad (7)$$

Where: LSTmax and LSTmin are maximum and minimum surface temperature in ^{o}C, respectively.

$$\text{LSTmax} = a_1 \text{ x NDVI} + b_1 \quad (8)$$

$$\text{LSTmin} = a_2 \times \text{NDVI} + b_2 \quad (9)$$

The empirical parameters a_1, a_2, b_1, and b_2 are found through linear-regression, representing the slope 'a' and intercept 'b' for both warm and cold edges of the data. The initial step in calculating SMI involves converting digital numbers to spectral radiance (L in W/m^2/sr/μm) using Eq. (10) (Lwin, 2010; Potic et al., 2017; Saha et al., 2019).

$$L = LSTmin + (((LSTmax - LSTmin)/ (QCALmax - QCALmin)) \times (\text{DN} - QCALmin)) \quad (10)$$

where: $LSTmin$ and $LSTmax$ are spectral radiance calibration constants (Table 1) and $QCALmax$ and $QCALmin$ denote the maximum and lowermost quantized calibration pixel values (Table 1).

Table 1: Spectral radiance and Quantized calibration pixel values for Landsat8 thermal bands (Potic et al., 2017; Saha et al., 2019)

	Band	Maximum radiance	Minimum radiance
Spectral radiance	4 and 5	1.3490	18.404
	10and 11	0.2004	19.002
Quantized calibration pixel	4 and 5	0.9900	286
	10 and 11	0.9900	59448

To compute $LSTmax$ and $LSTmin$, two inputs, namely LST and NDVI, were first estimated. The LST in Kelvin (K) is determined using Landsat 8 Thermal bands, employing Eq. (11) (Weng et al., 2004; Saha et al., 2019):

$$\text{LST} = Tb/ [1 + (\lambda \times Tb/C2) \times \ln(\varepsilon)] \quad (11)$$

where: Tb = Satellite Brightness Temp (Eq. (12), λ = wavelength of emitted radiance, $C2 = 1.4388 \times 10^{-2}$ m K, and ε = emissivity (typically 0.95)

$$Tb = (K_2/ (\ln (K_1 \times \varepsilon/\text{L} + 1))) \quad (12)$$

where: K_1 = calibration constant 1 depending on the sensor, K_2 = calibration constant 2 depending on the sensor (Table 2) and L = spectral radiance (Saha et al., 2019).

$$C2 = \text{h} \times \text{c/s} \quad (13)$$

where: h = 6.626×10^{-34} Js, c = light velocity = 2.998×10^{8} m/s, and s = constant from Boltzmann = 1.38×10^{-23} J/K.

Table 2: Thermal infrared constant for Landsat 8 (Potic et al., 2017; Lwin, 2010).

Thermal constant	Band 10	Band 11
K_1	774.8853	480.8883
K_2	1321.0789	1201.1442

2.5. Temperature vegetation dryness index (TVDI)

For evaluating drought situation locally, one of the appropriate index is to use TVDI; this was generated from NDVI and LST. TVDI reflects the surface soil moisture well, especially in broad areas with vegetation coverage and soil moisture. Eq. (14) was used to calculate TVDI from NDVI's land surface temperature (LST) (Carlson et al., 1994).

$$\text{TVDI} = \frac{\text{LST} - \text{LSTmin}}{\text{LSTmax} - \text{LSTmin}} \quad (14)$$

where LSTmax is max land surface temperature and LSTmin is min land surface temperature.

3. Results and Discussion

This study considered the years 2015 and 2021 in analyzing LST, SMI, and TVDI (Figures 3 and 4). In 2015, LST ranged from low to medium in the southern and southeastern parts of the study area. However, by 2021, these areas exhibited a spatial shift towards very high LST. Conversely, there was little change observed in the northern part of the study area. LST serves as a vital parameter for assessing evapotranspiration, vegetation water stress, soil moisture stress, and thermal inertia in the study region.

Figure 3 illustrates the spatial distribution of SMI in 2015, indicating predominantly low to medium values in the eastern and western parts of the study area, while the northern section showed predominantly high to very high values. Conversely, the spatial distribution of TVDI in 2015, exhibited a contrasting pattern to SMI, with predominantly very high to medium values in the eastern and western parts of the study area.

For both 2015 and 2021, the southern and eastern regions consistently displayed extreme LST, SMI, and TVDI patterns. According to Mitiku et al. (2022), the decrease in vegetation cover and increase in bare ground are correlated with rising LST. In our study area, there was a significant increase in both SMI and TVDI, indicating a direct correlation with LST.

In the study area, LST recorded in 2015 was relatively mild compared to that of 2021. Similarly, the resulting SMI and TVDI for 2015 were less severe compared to that of 2021. The significant increase in LST observed in 2021, accompanied by accelerated SMI and TVDI rates, can be attributed to the rising atmospheric temperatures during that period (Dessalegn et al., 2021; Mitiku et al., 2022).

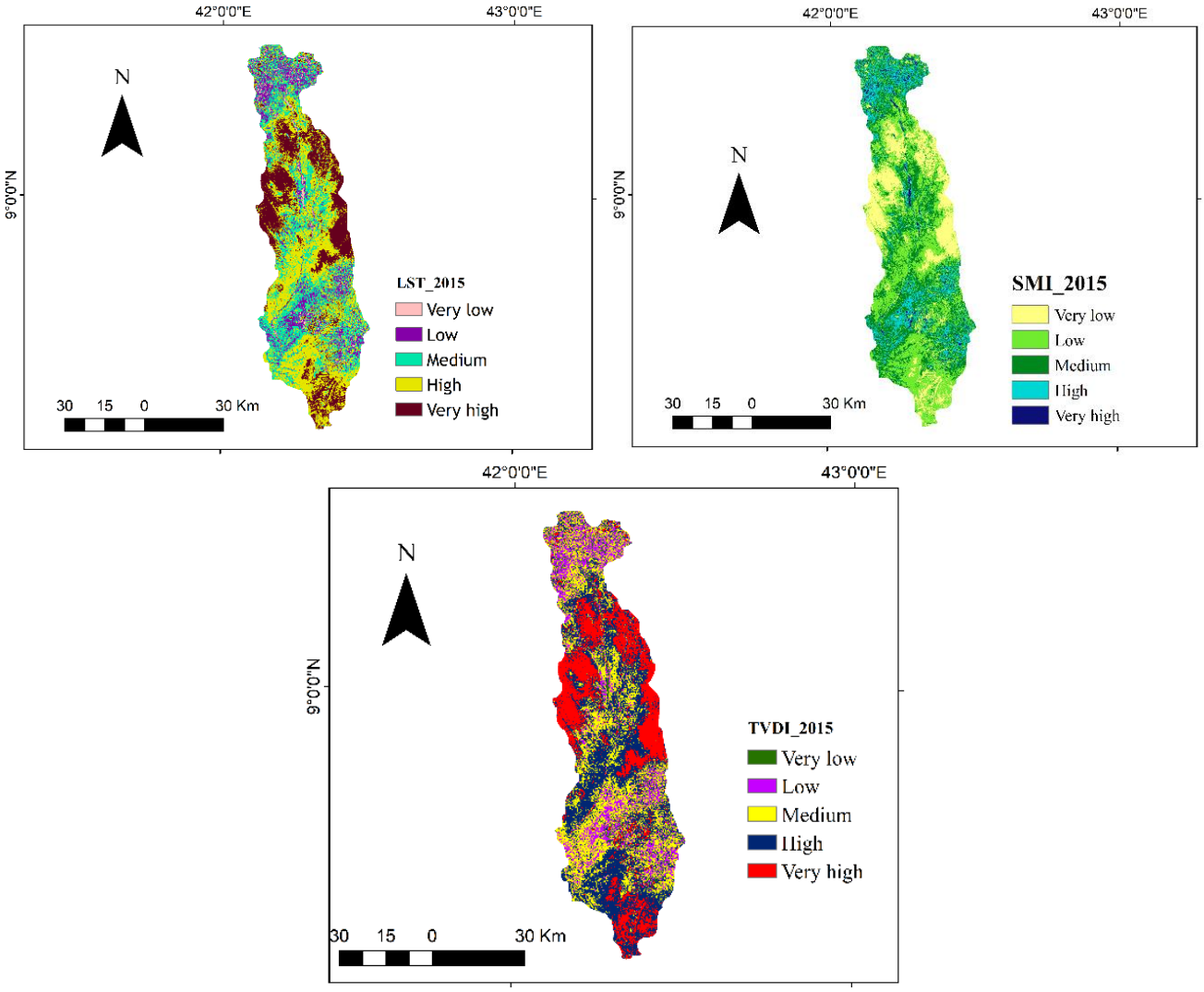

Figure 3: Spatial distribution of LST, SMI, and TVDI in 2015

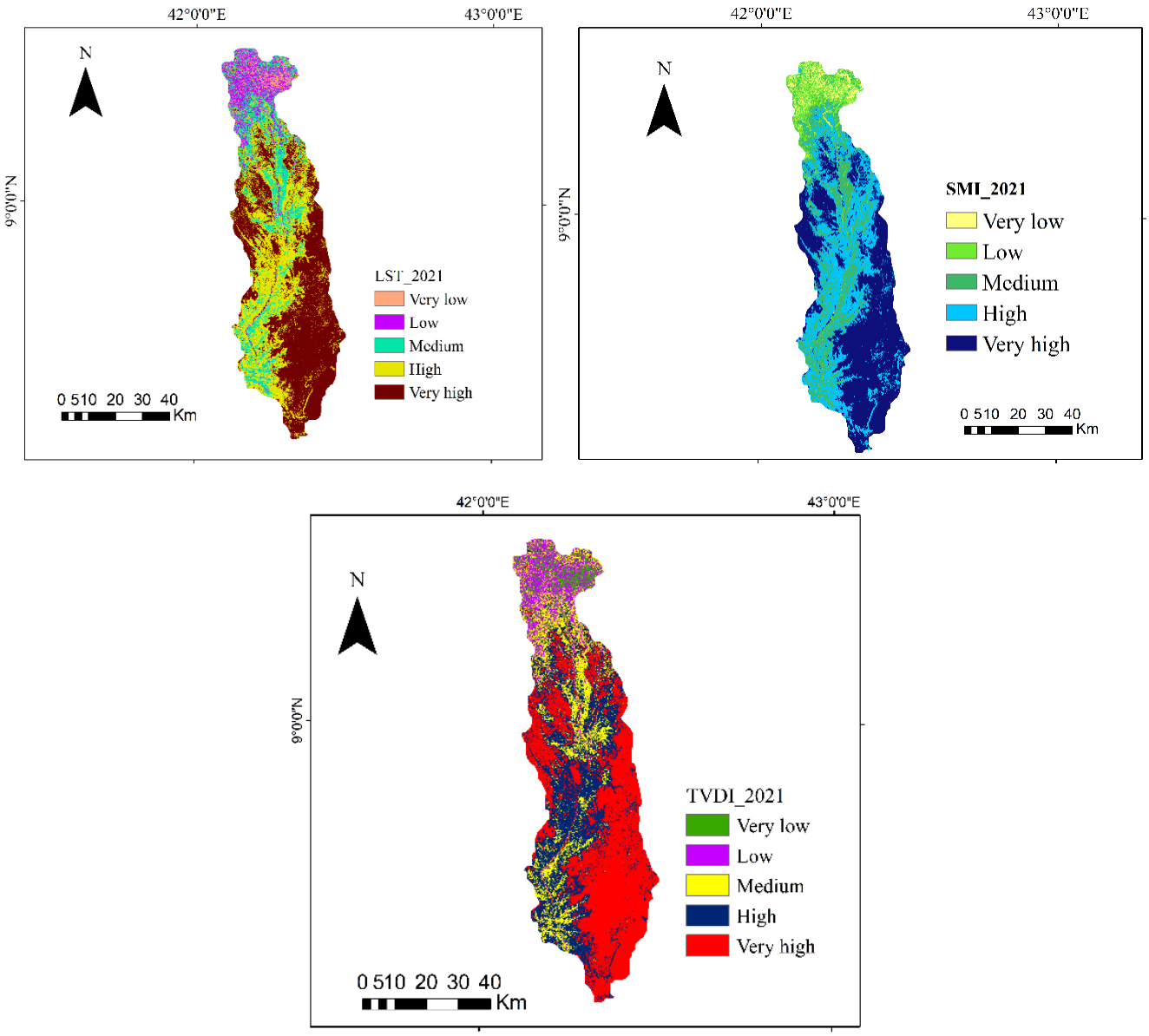

Figure 4: Spatial distribution of SMI, LST, and TVDI in 2021

The most notable finding was the substantial rise in LST in 2021, primarily driven by global warming, which impacts both atmospheric and LST trends positively. However, further analysis in this study revealed that the relationship between NDVI and LST played a crucial role in understanding the increase. It is important to note that spatially, LST increased in both 2015 and 2021, indicating a positive association with time as revealed by the study's results.

In a dry situation, neither transpiration nor evaporation occurs, resulting in very high spatial distributions of TVDI and SMI. Conversely, in wet conditions, both transpiration and evaporation reach their maximum levels, leading to very low TVDI and SMI values. Integrating LST and NDVI provides valuable insights into evapotranspiration, air temperature, and soil moisture content (Sandholt et al., 2002). TVDI and SMI parameters are closely linked to land cover characteristics, including LST and NDVI (Petropoulos et al., 2015). Theoretically, an inverse linear relationship between TVDI and soil moisture is proposed (Li et al., 2010).

This study focused on the understanding of the geographical and temporal relationships among Land LST, TVDI, and SMI in monitoring and assessing drought. Contrary to common belief, which suggests a

positive connection between LST, TVDI, and SMI, these variables are actually inversely related to soil moisture. This relationship is influenced by factors such as vegetation type, season, and geographic location, with various attempts made to explain it based on biophysical and geographic elements such as terrain, fractional vegetation cover, land-use land cover, and moisture conditions.

Generally, it was observed that an increase in LST often leads to a significant rise in TVDI and SMI. The study revealed a trend of increasing LST, SMI, and TVDI over time, contributing to soil moisture degradation. Specifically, the northeast and northwest regions of the Erer Watersheds exhibited the highest LST, SMI, and TVDI values, which are negatively correlated with soil moisture. Similarly, the Rift Valley of Ethiopia also displays a strong negative relationship between soil moisture and LST (Bayisa et al., 2022).

4. Conclusions and Recommendations

This study focused on the analysis of Land Surface Temperature, Soil Moisture Index, and Temperature Vegetation Dryness Index for the years 2015 and 2021. The results indicated a significant increase in LST from 2015 to 2021, particularly in the southern and southeastern parts of the study area. This rise in LST was accompanied by elevated SMI and TVDI values, suggesting a correlation between increasing atmospheric temperatures and soil moisture stress.

Furthermore, the study highlighted the intricate relationship between LST, TVDI, and SMI, revealing a pattern of increasing soil moisture deficit over time. The spatial distribution of these indices demonstrated geographical variations, with certain regions consistently exhibiting higher LST, SMI, and TVDI values, indicative of severe soil moisture stress. The study identified an inverse relationship between LST, TVDI, and SMI, emphasizing the complex interplay of factors such as vegetation type, seasonality, and geographic location. This finding underscores the importance of considering multiple variables and environmental factors when assessing drought conditions and soil moisture dynamics.

Continuation of long-term monitoring efforts is essential to track trends in LST, SMI, and TVDI over extended periods. The longitudinal approach will provide valuable insights into the dynamics of soil moisture stress and climate change impacts on the study area. Incorporating additional remote sensing datasets, such as precipitation records and land cover classifications, can enhance the accuracy of drought monitoring and prediction models. Integrating multi-source data will also improve the understanding of the complex interactions between climate variables and soil moisture dynamics. Conducting localized assessments at finer spatial scales can capture microclimate variations and better inform targeted adaptation and mitigation strategies. This approach will enable stakeholders to address specific soil moisture stress hotspots and prioritize resource allocation for drought resilience measures. Policymakers are suggested to consider integrating scientific findings into land use planning and water resource management strategies. Implementing evidence-based policies that promote sustainable land management practices and water conservation measures can help mitigate the impacts of soil moisture stress and climate change on agricultural productivity and ecosystem health.

Acknowledgments: The authors are grateful to Haramaya and Woldia Universities for the staff time allocated to this research work. The authors would also like to express their deepest thanks to the anonymous reviewers for their time and valuable professional comments that have enriched the manuscript.

Reference

Ali, R. R. & Shalaby, A. (2012). Response of topsoil features to the seasonal changes of land surface temperature in the arid environment. *International Journal of Soil Science*, 7(2), 39–50.

Amani, M., Salehi, B., Mahdavi, S., Masjedi, A. & Dehnavi, S. (2017). Temperature-vegetation-soil moisture dryness index (TVMDI). *Remote Sensing of Environment*, 197, 1-14.

Anderson, K., & Croft, H. (2009). Remote sensing of soil surface properties. *Progress in Physical Geography: Earth and Environment*, 33(4), 457-473.

Avdan, U., & Jovanovska, J. (2016). Algorithm for automated mapping of lLand surface temperature uUsing LANDSAT 8 satellite data. *Journal of Sensors*, 1480307.

Barsi, J. A., Lee, K., Kvaran, G., Markham, B. L. & Pedelty, J. A. (2014). The sSpectral sesponse of the landsat-8 operational land imager. *Remote Sensing*, 6, 10232-10251.

Bayisa Negasa Wolteji, Sintayehu Teka Bedhadha, Sintayehu Legese Gebre, Esayas Alemayehu & Dessalegn Obsi Gemeda (2022). Multiple Indices based agricultural drought assessment in the Rift Valley Region of Ethiopia. *Environmental Challenges*, 7, 100488.

Carlson, T. N., Gillies, R. R. & Perry, E. M. (1994). A method to make use of thermal infrared temperature and NDVI measurements to infer surface soil water content and fractional vegetation cover. *Remote sensing reviews*, 9(1-2), 161-173.

Chen, X. & Zhang, Y. (2017). Impacts of urban surface characteristics on spatiotemporal pattern of land surface temperature in Kunming of China. *Sustainable Cities and Society*, 32, 87-99.

Das, M., Das, A. & Momin S. (2022). Quantifying the cooling effect of urban green space: A case from urban parks in a tropical mega metropolitan area (India). *Sustainable Cities and Society*, 87, 104062.

Dessalegn Obsi Gemeda, Debela Hunde Feyssa & Weyessa Garedew (2021). Meteorological data trend analysis and local community perception towards climate change: a case study of Jimma City, Southwestern Ethiopia. *Environment, Development and Sustainability*, 23, 5885-5903.

Dissanayake, D., Morimoto, T., Ranagalage, M. & Murayama, Y. (2019). Land-uUse/land-cover cChanges and their impact on surface urban heat islands: case study of Kandy City, Sri Lanka. *Climate*, 7(8), 99.

Dobriyal, P., Qureshi, A., Badola, R. & Ainul Hussain S. (2012). A review of the methods available for estimating soil moisture and its implications for water resource management. *Journal of Hydrology*, 458-459, 110-117.

He, S. & Wu, J. (2019). Relationships of groundwater quality and associated health risks with land use/land cover patterns: A case study in a loess area, Northwest China. *Human and Ecological Risk Assessment: International J.*, 25(1-2), 354-373.

Jimenez-Munoz, J. C., Sobrino, J. A., Gillespie, A., Sabol, D. & Gustafson, W. T. (2006). Improved land surface emissivities over agricultural areas using ASTER NDVI. *Remote Sensing of Environment*, 103(4), 474-487.

Joiner, J. Yoshida, Y. Anderson, M., Holmes, T. Hain, C. Reichle, R. Koster, R. Middleton, E. & Zeng, F. (2019). Global relationships among traditional reflectance vegetation indices (NDVI and NDII), evapotranspiration (ET), and soil moisture variability on weekly timescales. *Remote Sensing of Environment*, 219, 339-352.

Khandelwal, S., Goyal, R., Kaul, N. & Mathew, A. (2018). Assessment of land surface temperature variation due to change in elevation of area surrounding Jaipur, India. *The Egyptian Journal of Remote Sensing and Space Science*, 21(1), 87–94.

Li, H., Li, C., Lin Y. & uping, Lei Y. (2010). Surface temperature correction in TVDI to evaluate soil moisture over a large area. *Journal of Food, Agriculture & Environment* , 8(3&4), 1141-1145.

Li, Z., Leng, P., Zhou, C., , K., Zhou, F. & Shang, G. (2021). Soil moisture retrieval from remote sensing measurements: Current knowledge and directions for the future. *Earth-Science Reviews*, 218, 103673.

Liang, Y., Li, Y., Wang, H., Zhou, J., Wang, J., Regier, T. & Dai, H. (2011). Co_3O_4 nanocrystals on graphene as a synergistic catalyst for oxygen reduction reaction. *Nature materials*, 10, 780-786.

Liu, Y. Y., Dorigo, W. A., Parinussa, R. M., de Jeu, R. A., Wagner, W., McCabe, M. F., Evans, J. P. & Van Dijk, A. I. (2012). Trend-preserving blending of passive and active microwave soil moisture retrievals. *Remote Sens. Environ.*, 123, 280-297.

Lu, D. & Weng, Q. (2004). Spectral mixture analysis of the urban landscape in Indianapolis with Landsat ETM+ imagery. *Photogrammetric Engineering & Remote Sensing*, 70(9), 1053–1062.

Lwin, K. (2010). *Estimation of landsat TM surface temperature using ERDAS imagine spatial modeler; SIS tutorial series*. Retrieved from http://giswin.geo.tsukuba.ac.jp/sis/tutorial/koko/SurfaceTemp/SurfaceTemperature.pdf

Mallick, J., Kant, Y. & Bharath, B. D. (2008). Estimation of land surface temperature over Delhi using Landsat-& ETM+. *J. Ind. Geophys. Union,* , 12(3), 131–140.

Mitiku Badasa Moisa, Biratu Bobo Merga & Dessalegn Obsi Gemeda (2022). Multiple indices-based assessment of agricultural drought: A case study in Gilgel Gibe Sub-basin, Southern Ethiopia. *Theoretical and Applied Climatology*, 148, 455-464.

MoA (2000). *Agro-ecological zonations of Ethiopi*a. Minstry of Agriculture, Addis Ababa, Ethiopia.

Mohamed., E. S., Ali, A. M., El-Shirbeny, M. A., Abutaleb, K. A. & Shaddad, S. M. (2020). Mapping soil moisture and their correlation with crop pattern using remotely sensed data in arid region. *Egypt. J. Remote Sens. Space Sci.*, 23(3), 347-353.

Petropoulos, G. P., Ireland, G. & Barrett, B. (2015). Surface soil moisture retrievals from remote sensing: current status, products & future trends. *Physics and Chemistry of the Earth Parts A/B/C*, 83-84, 36-56.

Phan, T. N., Kappas, M. & Tran, T. P. (2018). Land surface temperature variation due to changes in elevation in Northwest Vietnam. *Climate, 6*(2), 28.

Potic, I., Bugarski, M. & Matic-Varenica, J. (2017). Soil moisture determination using remote sensing data for the property protection and increase of agriculture production. *In Proceedings of the 2017 Annual World Bank Conference on Land and Poverty*. Washington, DC, March 20-24, 2017.

Rahman, H. & Dedieu, G. (1994). A simplified method for the atmospheric correction of satellite measurements in the solar spectrum. *International Journal of Remote Sensing*, 15(1), 123–143.

Rouse, J. W., Haas, R. H., Schell, J. A., Deering, D. W. & Harlan, J. C. (1974). *Monitoring the vernal advancements (greenwave effect) and retrogradation of natural vegetation, NASA/GSFCT type III final report,* Texas A & M University, Remote Sensing Center, College Station, pp. 1-137.

Saha, A., Patil, M., Goyal, V., & Rathore, D. (2019). Assessment and impact of soil moisture index in agricultural drought estimation using remote sensing and GIS techniques. *Proceedings*, 7(1), 2.

Sandholt, I., Rasmussen, K. & Andersen, J. (2002). A simple interpretation of the surface temperature/vegetation index space for assessment of surface moisture status. *Remote Sensing of Environment*, 79(2-3), 213-224.

Schnur, M. T., Xie, H. & Wang, X. (2010). Estimating root zone soil moisture at distant sites using MODIS NDVI and EVI in a semi-arid region of southwestern USA. *Ecological Informatics*, 5(5), 400-409.

Shumete, Y. (2015). *Ethiopia - Land degradation neutrality national report, United Nations Convention to combat desertification*. France. Retrieved from https://policycommons.net/artifacts/1996031/federal-democratic-republic-of-ethiopia-ethiopia/2747796/fragments/ on 17 Apr 2024. CID: 20.500.12592/4njvkg.

Sobrino, J. A. & Raissouni, N. (2000). Toward remote sensing methods for land cover dynamic monitoring: Application to Morocco. *International Journal of Remote Sensing*, 21(2), 353-366.

Sobrino., J. A., Jimenez-Munoz., J. C. & Paolini, L. (2004). Land surface temperature retrieval from LANDSAT TM 5. *Remote Sensing of Environment,* , 90(4), 434-440.

Song, Z., Yang, H., Huang, X., Yu, W., Huang, J. & Ma, M. (2021). The spatiotemporal pattern and influencing factors of land surface temperature change in China from 2003 to 2019. *International Journal of Applied Earth Observation and Geoinformation*, 104, 102537.

Sun, D. & Pinker, R. T. (2003). Estimation of land surface temperature from a geostationary operational environmental satellite (GOES-8). *Journal of Geophysical Research: Atmospheres,* 108(D11), 4326.

USGS (2021). *Landsat missions: Using the U.S. geological survey landsat level-1 data product*. Retrieved from https://www.usgs.gov/core-science-systems/nli/landsat/using-usgs-landsat-level-1-data-product

Vlassova, L., Perez-Cabello, F., Mimbrero, M. R, Lloveria, R. M. & Garcia-Martín, A. (2014). Analysis of the relationship between land surface temperature and wildfire severity in a series of landsat images . *Remote Sensing*, 6, 6136-6162.

Wan, Z., Zhang, Y., Zhang, Q. & Li, Z.-L. (2004). Quality assessment and validation of the MODIS global land surface temperature. *International Journal of Remote Sensing*, 25(1), 261-274.

Weng, Q. (2009). Thermal remote sensing of urban climate and environmental studies: methods, applications, and trends. *ISPRS Journal of Photogrammetry and Remote Sensing*, 64(4), 335-344.

Weng, Q., Lu, D., & Schubring, J. (2004). Estimation of land surface temperature–vegetation abundance relationship for urban heat island studies. *Remote Sensing of Environment*, 89(4), 467–483.

Yang, T., Ala, M., Zhang, Y., Wu, J., Wang, A. & Guan, D. (2018). Characteristics of soil moisture under different vegetation coverage in Horqin Sandy Land, Northern China. *PLoS One*, 13(6), e0198805

Yuan, F. & Bauer, M. E. (2007). Comparison of impervious surface area and normalized difference vegetation index as indicators of surface urban heat island effects in Landsat imagery. *Remote Sensing of environment*, 106(3), 375-386.

Zullo, F., Fazio, G., Romano, B., Marucci, A. & Fiorini, L. (2019). Effects of urban growth spatial pattern (UGSP) on the land surface temperature (LST): A study in the Po Valley (Italy). *Science of The Total Environment*, 650(part 2), 1740-1751.